SUPPLEMENTAL INFORMATION

REFERENCES CONT.

51. Gao, J. *et al.* Integrative analysis of complex cancer genomics and clinical profiles using the cBioPortal. *Sci. Signal.* (2013) doi:10.1126/scisignal.2004088.

52. You, S. *et al.* Integrated classification of prostate cancer reveals a novel luminal subtype with poor outcome. *Cancer Res.* (2016) doi:10.1158/0008-5472.CAN-16-0902.

53. Plantinga, M. J. *et al.* Telomerase suppresses formation of ALT-associated single-stranded telomeric C-circles. *Mol. Cancer Res.* (2013) doi:10.1158/1541-7786.MCR-13-0013.

54. D'Adda Di Fagagna, F. *et al.* A DNA damage checkpoint response in telomere-initiated senescence. *Nature* (2003) doi:10.1038/nature02118.

55. Debacq-Chainiaux, F., Erusalimsky, J. D., Campisi, J. & Toussaint, O. Protocols to detect senescence-associated beta-galactosidase (SA-βgal) activity, a biomarker of senescent cells in culture and in vivo. *Nat. Protoc.* (2009) doi:10.1038/nprot.2009.191.

56. Brown, J. P., Wei, W. & Sedivy, J. M. Bypass of senescenoe after disruption of p21(CIP1)/(WAF1) gene in normal diploid human fibroblasts. *Science (80-.).* (1997) doi:10.1126/science.277.5327.831.

57. Beltran, H. *et al.* Challenges in recognizing treatment-related neuroendocrine prostate cancer. *J. Clin. Oncol.* (2012) doi:10.1200/JCO.2011.41.5166.

58. KOMIYA, A. *et al.* The prognostic significance of loss of the androgen receptor and neuroendocrine differentiation in prostate biopsy specimens among castration-resistant prostate cancer patients. *Mol. Clin. Oncol.* (2013) doi:10.3892/mco.2013.69.

59. Shen, R. *et al.* Transdifferentiation of cultured human prostate cancer cells to a neuroendocrine cell phenotype in a hormone-depleted medium. *Urol. Oncol.* (1997) doi:10.1016/S1078-1439(97)00039-2.

60. Burchardt, T. *et al.* Transdifferentiation of prostate cancer cells to a neuroendocrine cell phenotype in vitro and in vivo. *J. Urol.* (1999) doi:10.1016/S0022-5347(05)68241-9.

61. Pernicová, Z. *et al.* The role of high cell density in the promotion of neuroendocrine

transdifferentiation of prostate cancer cells. *Mol. Cancer* (2014) doi:10.1186/1476-4598-13-113.

62. Ather, M. H., Abbas, F., Faruqui, N., Israr, M. & Pervez, S. Correlation of three immunohistochemically detected markers of neuroendocrine differentiation with clinical predictors of disease progression in prostate cancer. *BMC Urol.* (2008) doi:10.1186/1471-2490-8-21.
63. Kim, J. *et al.* FOXA1 inhibits prostate cancer neuroendocrine differentiation. *Oncogene* (2017) doi:10.1038/onc.2017.50.
64. Bluemn, E. G. *et al.* Androgen Receptor Pathway-Independent Prostate Cancer Is Sustained through FGF Signaling. *Cancer Cell* (2017) doi:10.1016/j.ccell.2017.09.003.
65. Kregel, S. *et al.* Acquired resistance to the second-generation androgen receptor antagonist enzalutamide in castration-resistant prostate cancer. *Oncotarget* (2016) doi:10.18632/oncotarget.8456.
66. Brault, M. E. & Autexier, C. Telomeric recombination induced by dysfunctional telomeres. *Mol. Biol. Cell* (2011) doi:10.1091/mbc.E10-02-0173.
67. Cesare, A. J. *et al.* Spontaneous occurrence of telomeric DNA damage response in the absence of chromosome fusions. *Nat. Struct. Mol. Biol.* (2009) doi:10.1038/nsmb.1725.
68. Guervilly, J. H. *et al.* The SLX4 complex is a SUMO E3 ligase that impacts on replication stress outcome and genome stability. *Mol. Cell* (2015) doi:10.1016/j.molcel.2014.11.014.
69. Liu, S. *et al.* Telomerase as an important target of androgen signaling blockade for prostate cancer treatment. *Mol. Cancer Ther.* (2010) doi:10.1158/1535-7163.MCT-09-0924.
70. Moehren, U. *et al.* Wild-type but not mutant androgen receptor inhibits expression of the hTERT telomerase subunit: A novel role of AR mutation for prostate cancer development. *FASEB J.* (2008) doi:10.1096/fj.07-9360com.
71. Li, Y. & Tergaonkar, V. Noncanonical functions of telomerase: Implications in telomerase-targeted cancer therapies. *Cancer Research* (2014) doi:10.1158/0008-5472.CAN-13-3568.
72. Morgenstern, J. P. & Land, H. Advanced mammalian gene transfer: High titre retroviral vectors with multiple drug selection markers and a complementary helper-free packaging cell line. *Nucleic Acids Res.* (1990) doi:10.1093/nar/18.12.3587.
73. Dull, T. *et al.* A Third-Generation Lentivirus Vector with a Conditional Packaging System. *J. Virol.*

(1998) doi:10.1128/jvi.72.11.8463-8471.1998.

74. Popovics, P. *et al.* Prostatic osteopontin expression is associated with symptomatic benign prostatic hyperplasia. *bioRxiv* (2019).

75. Zeng, X. *et al.* Administration of a Nucleoside Analog Promotes Cancer Cell Death in a Telomerase-Dependent Manner. *Cell Rep.* (2018) doi:10.1016/j.celrep.2018.05.020.

76. Hou, M., Xu, D., Björkholm, M. & Gruber, A. Real-time quantitative telomeric repeat amplification protocol assay for the detection of telomerase activity. *Clin. Chem.* (2001).

A.

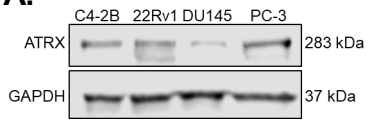

B.

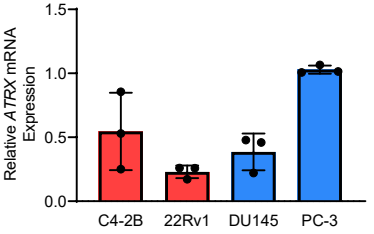

Supplemental Figure 1: (A) Relative ATRX protein expression across CRPC cell lines. **(B)** Relative *ATRX* mRNA expression across CRPC cell lines. Data represented as mean±SD; n=3; *p<0.05; **p<0.01; ***p<0.001; ****p<0.0001.

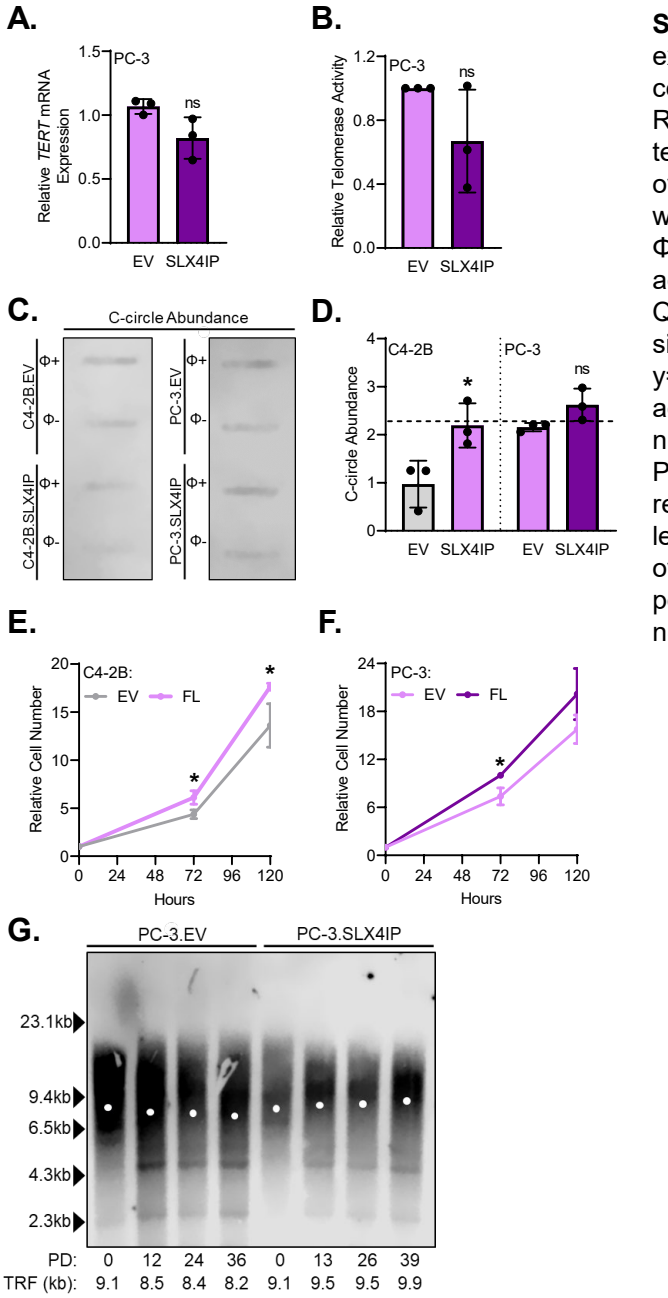

Supplemental Figure 2: (A) Relative *TERT* mRNA expression and **(B)** relative telomerase activity in PC-3 cells with stable SLX4IP overexpression. **(C)** Representative dot blot demonstrating the presence of telomeric C-circles in C4-2B and PC-3 cells with SLX4IP overexpression. Φ+ lane indicates reactions incubated with Φ29 polymerase for telomeric C-circle amplification. Φ- lane indicates control reaction lacking polymerase to account for background telomeric signal. **(D)** Quantification of C-circle abundance defined as the signal ratio of Φ+ reaction to Φ- reaction. Dotted line at y=2 indicates threshold signal ratio suggesting ALT activity. **(E)** Using trypan blue exclusion, relative cell number was followed over 120 hours for C4-2B and **(F)** PC-3 cells with SLX4IP overexpression. **(G)** Telomere restriction fragment analysis demonstrating telomere length changes over 45 days in PC-3 cells overexpressing SLX4IP versus control. PD: Calculated population doublings. Data represented as mean±SD; n=3; *p<0.05; **p<0.01; ***p<0.001; ****p<0.0001.

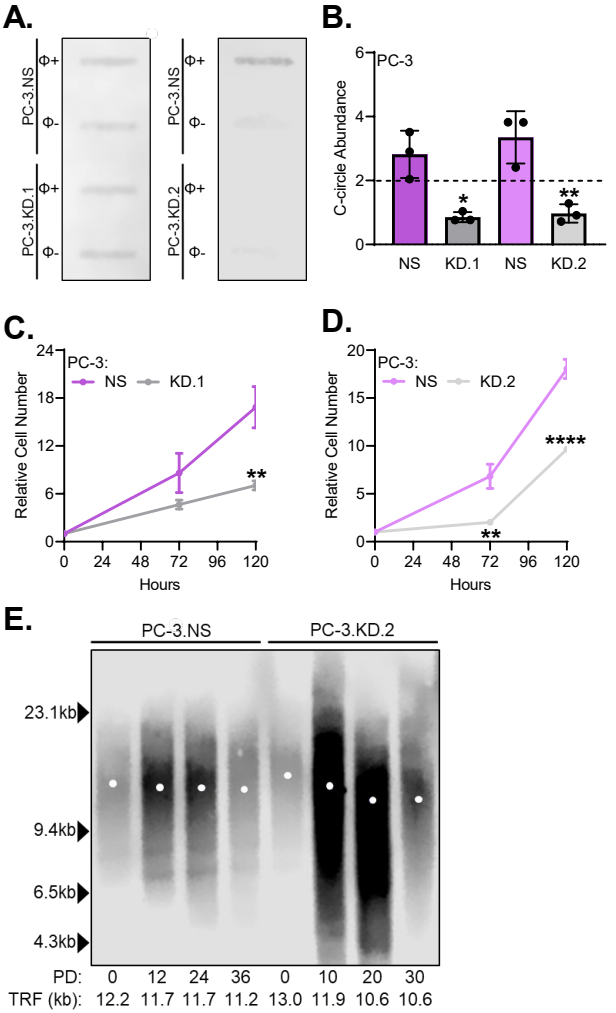

Supplemental Figure 3: (A) Representative dot blot demonstrating the presence of telomeric C-circles in PC-3 cells with SLX4IP knockdown. Φ+ lane indicates reactions incubated with Φ29 polymerase for telomeric C-circle amplification. Φ- lane indicates control reaction lacking polymerase to account for background telomeric signal. **(B)** Quantification of C-circle abundance defined as the signal ratio of Φ+ reaction to Φ- reaction. Dotted line at y=2 indicates threshold signal ratio suggesting ALT activity. **(C)** Using trypan blue exclusion, relative cell number was followed over 120 hours in PC-3.NS versus KD.1 or **(D)** KD.2 cells. **(E)** Telomere restriction fragment analysis demonstrating telomere length changes over 45 days in PC-3 cells with SLX4IP knockdown (KD.2) versus control. PD: Calculated population doublings. Data represented as mean+SD; n=3; *p<0.05; **p<0.01; ***p<0.001; ****p<0.0001.

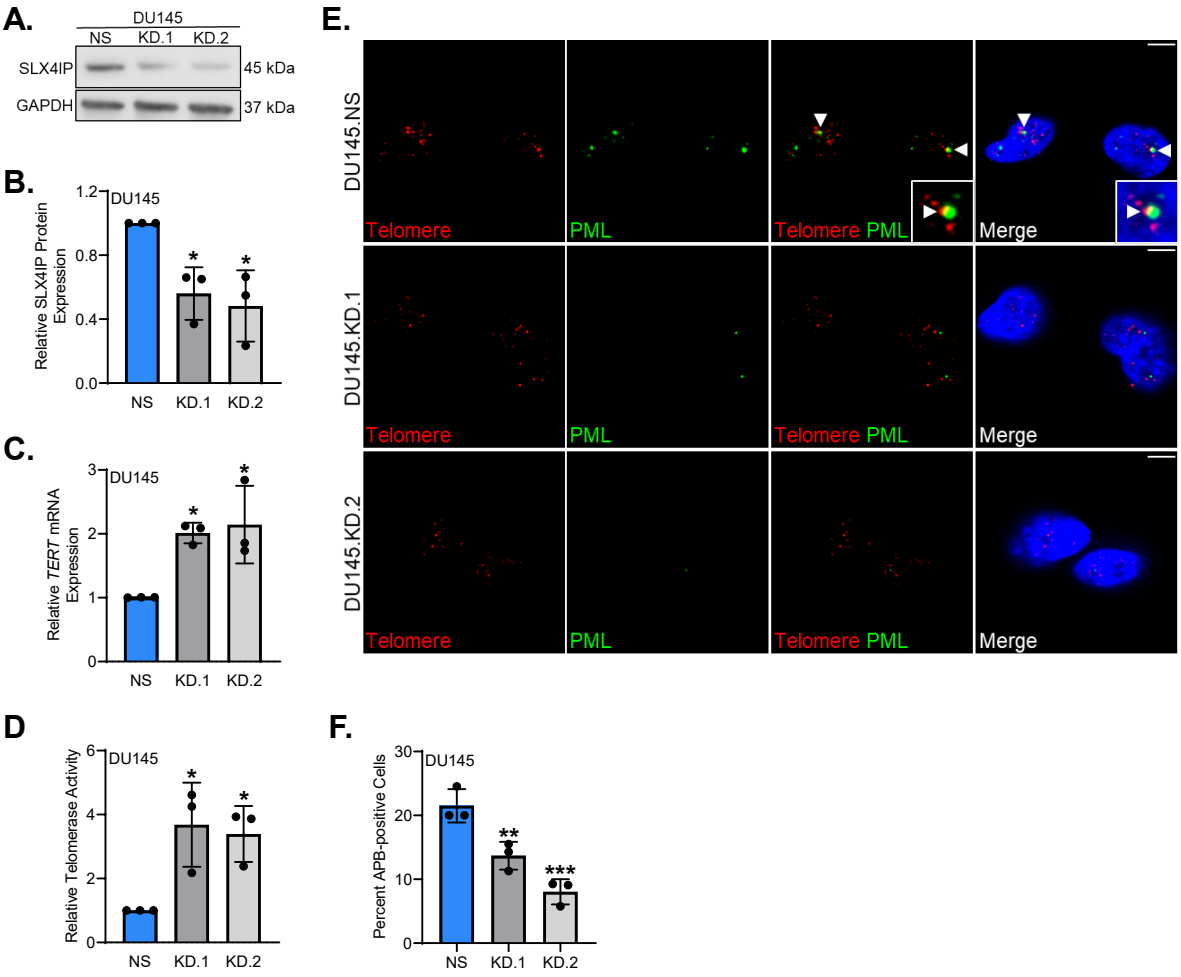

Supplemental Figure 4: (A) Confirmation of stable SLX4IP knockdown using two shRNAs (KD.1, KD.2) in DU145 cells with scrambled shRNA control (NS) at the protein level. **(B)** Quantification of (A). **(C)** Relative *TERT* mRNA expression and **(D)** relative telomerase activity following SLX4IP knockdown in DU145 cells. **(E)** Representative IF-FISH images demonstrating the presence or absence of APBs at telomeres (arrowheads) in DU145 cells with SLX4IP knockdown. Scale bar: 5 μm. **(F)** Quantification of IF-FISH images for percent APB-positive cells. Data represented as mean+SD; n=3; *p<0.05; **p<0.01; ***p<0.001; ****p<0.0001.

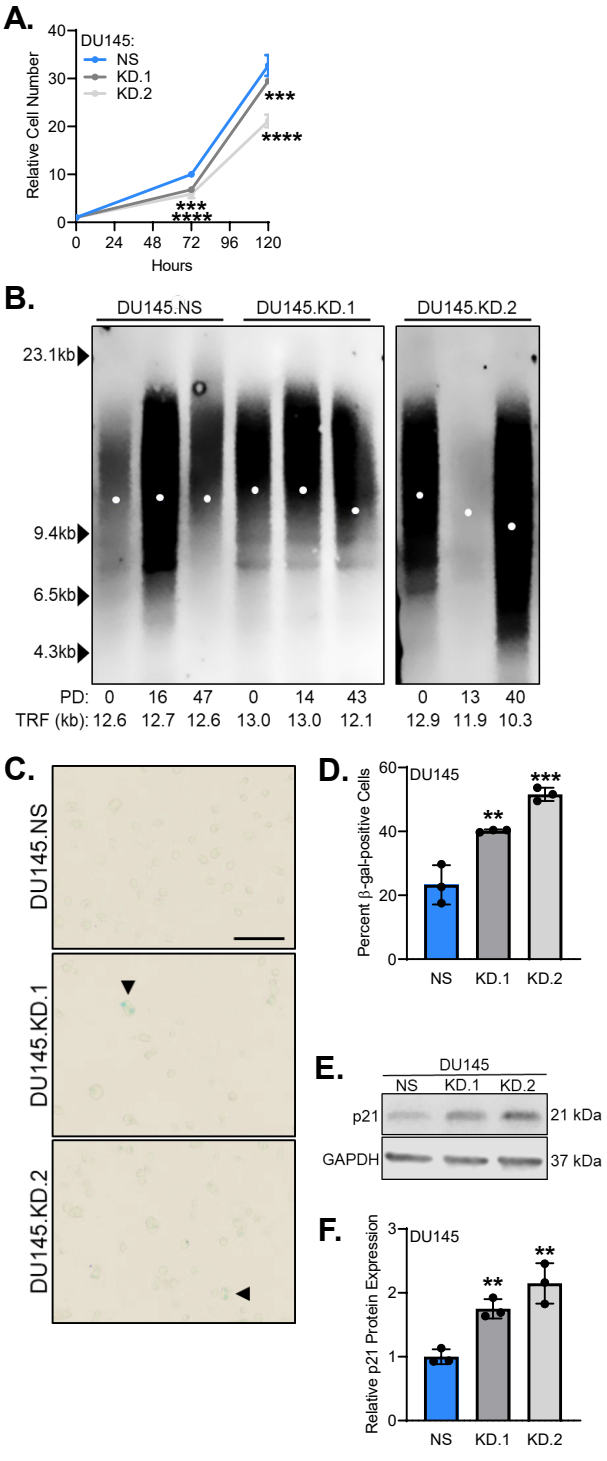

Supplemental Figure 5: (A) Using trypan blue exclusion, relative cell number was followed over 120 hours for DU145 cells with SLX4IP knockdown (KD.1, KD.2). **(B)** Telomere restriction fragment analysis demonstrating telomere length changes over 45 days in DU145 cells with SLX4IP knockdown (KD.1, KD.2) versus control. PD: Calculated population doublings. **(C)** Representative bright field images demonstrating β-galactosidase staining (arrowheads) for senescence in DU145 cells with stable knockdown of SLX4IP. Scale bar: 20 μm. **(D)** Quantification of (C). **(E)** Relative p21 expression following knockdown of SLX4IP in DU145 cells. **(F)** Quantification of (E). Data represented as mean±SD; n=3; *p<0.05; **p<0.01; ***p<0.001; ****p<0.0001.

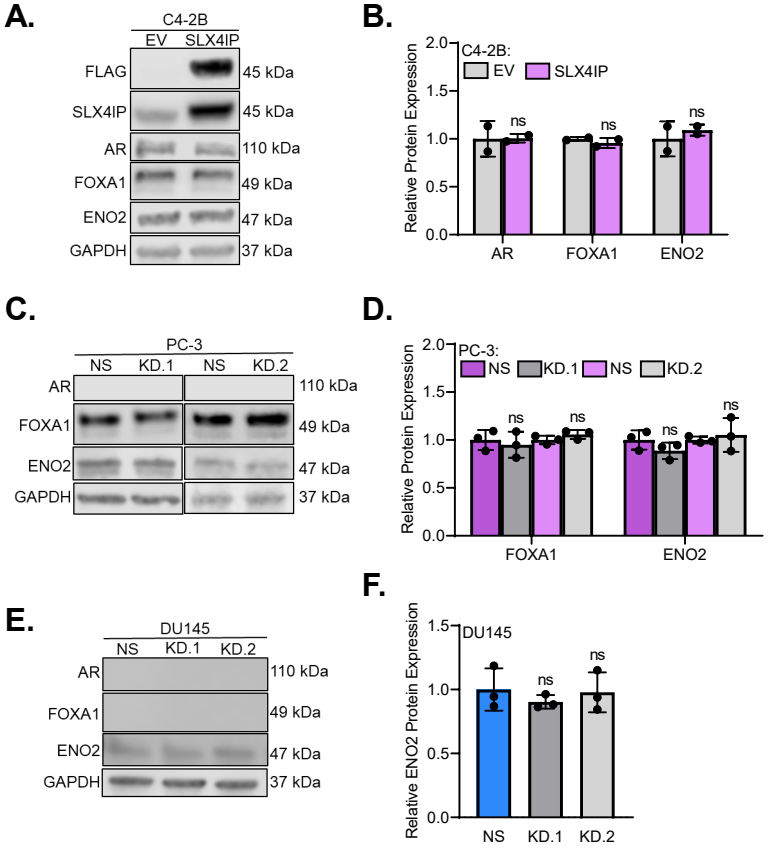

Supplemental Figure 6: (A) Changes in AR, FOXA1, and ENO2 protein expression in C4-2B transiently overexpressing SLX4IP. n=2 **(B)** Quantification of (A). **(C)** Changes in AR, FOXA1 and ENO2 protein expression in PC-3 cells with stable knockdown of SLX4IP. **(D)** Quantification of (C). **(E)** Changes in AR, FOXA1 and ENO2 protein expression in DU145 cells with stable knockdown of SLX4IP. **(F)** Quantification of (E) Data represented as mean±SD; n=3; *p<0.05; **p<0.01; ***p<0.001; ****p<0.0001.